



HAL
open science

Core-shell structure of chemically synthesised FePt nanoparticles: a comparative study

Michael Delalande, Pierre R. Marcoux, Peter Reiss, Yves Samson

► **To cite this version:**

Michael Delalande, Pierre R. Marcoux, Peter Reiss, Yves Samson. Core-shell structure of chemically synthesised FePt nanoparticles: a comparative study. *Journal of Materials Chemistry*, 2007, 17 (16), pp.1579-1588. 10.1039/b614209e . cea-02528443

HAL Id: cea-02528443

<https://cea.hal.science/cea-02528443>

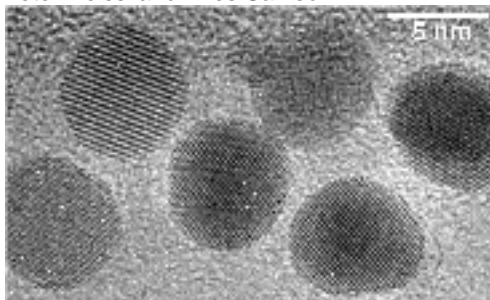
Submitted on 1 Apr 2020

HAL is a multi-disciplinary open access archive for the deposit and dissemination of scientific research documents, whether they are published or not. The documents may come from teaching and research institutions in France or abroad, or from public or private research centers.

L'archive ouverte pluridisciplinaire **HAL**, est destinée au dépôt et à la diffusion de documents scientifiques de niveau recherche, publiés ou non, émanant des établissements d'enseignement et de recherche français ou étrangers, des laboratoires publics ou privés.

Core-shell structure of chemically synthesised FePt nanoparticles: a comparative study

Michaël Delalande, Pierre R. Marcoux, Peter Reiss and Yves Samson



We conducted a comparative study about solution synthesis of FePt nanoparticles through different chemical processes, using four "hot soap methods" and one polyol process.

Core-shell structure of chemically synthesised FePt nanoparticles: a comparative study†

Michaël Delalande,^a Pierre R. Marcoux,^b Peter Reiss^{*b} and Yves Samson^{*a}

Receipt/Acceptance Data [DO NOT ALTER/DELETE THIS TEXT]

10 Publication data [DO NOT ALTER/DELETE THIS TEXT]

DOI: 10.1039/b000000x [DO NOT ALTER/DELETE THIS TEXT]

We carried out solution synthesis of FePt nanoparticles through different chemical methods, using four “hot soap methods”, i.e. the particle formation in the presence of surfactant molecules at high temperatures, and one polyol process. Structural and magnetic properties of the as-made particles pointed to a core-shell structure for the particles prepared with hot soap methods, with an iron-depleted core surrounded by a pure iron shell. Such a structure has an impact on the magnetic properties of as-made particles since Fe atoms from shell are oxidised and non magnetic. We proved however that iron atoms of this shell are available during the formation of the ordered phase upon annealing: L1₀ phase for small particles, L1₂ for bigger ones. In contrast, the core-shell structure was not observed in the case of nanoparticles synthesised according to the polyol process. This outlines the key role of the stabilising ligands, long alkyl chain surfactants in the former case and tetraethylene glycol in the latter.

Introduction

Chemical methods have been widely used to produce nanosized materials due to their straightforward nature and their potential to prepare large quantities of the final product.¹ Furthermore, they provide particles that are easily dispersible in liquid media, and therefore give the opportunity to fabricate nanostructured devices through self-assembly.²

The synthesis of discrete magnetic nanoparticles with sizes ranging from 2 to 20 nm is of significant importance, because of their applications in Tbit.in⁻² magnetic storage devices³ and in biotechnologies.⁴ The superparamagnetism limit makes it necessary to use highly anisotropic materials. Among magnetic metallic alloys, the FePt alloy in the L1₀ phase is a prominent candidate. This ordered phase has indeed a very high uniaxial anisotropy, $K_u = 7 \times 10^6$ J/m³, so that the critical diameter, below which thermal fluctuations induce random switching of the magnetisation direction, is as small as 3.5 nm.

For this reason, many processes for the chemical synthesis of nanometer-sized FePt nanoparticles have been developed. First of all these reactions aim at monodisperse particles, in order to facilitate subsequent self-assembly, and to yield homogeneous magnetic properties of particles. Secondly, these reactions should provide size-tunable particles, with a diameter large enough compared to the critical diameter. Thirdly, the stoichiometry should be as close to Fe₅₀Pt₅₀ as possible since the chemically ordered L1₀ phase, with a high

50 magnetocrystalline anisotropy, includes as many Fe atoms as Pt atoms. Finally, the as-made particles should be readily dispersible in common solvents, because self-assembly phenomena are sensitive to aggregation. Furthermore, in some cases size-selection steps are necessary and such processes require also a good solubility. The first reported protocol mentioned in 2000 the synthesis of FePt nanoparticles in a high-boiling coordinating solvent. It was later called “hot soap method” since the formation of metallic Fe and Pt atoms was performed in presence of surfactant molecules.⁵ A similar method was subsequently extended to the synthesis of another binary alloy (CoPt),⁶ and then to ternary alloys (FePtAg).⁷

Most of the solution synthesis methods of FePt nanoparticles are based on the transformation of an iron precursor and a platinum precursor into the metallic state, in presence of two surfactant molecules (one that preferentially binds to Fe surface atoms, another one for Pt). The latter are in charge with stabilising metallic nuclei in solution by preventing aggregation during growth. Precursors may be either organometallic (Fe⁰ in iron pentacarbonyl for example) or ionic (*e. g.* Pt^{II} in platinum acetylacetonate). The use of an oxidised metal as a precursor implies the presence of a reducing agent, a strong one if Fe^{II} and Pt^{II} have to be reduced,⁸ a milder one if just Pt^{II} needs to be reduced. Due to their higher reduction potential (1.2 V vs. -0.4 V), platinum salts can easier be reduced as compared to iron salts. In some cases, the reducing agent may be the solvent,⁹ or one of the metallic precursors.¹⁰ As a conclusion, let us notice that there are very few hot soap reactions involving an organometallic Pt⁰ precursor.

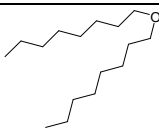
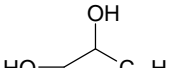
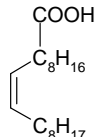
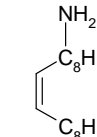
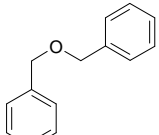
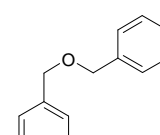
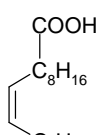
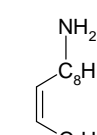
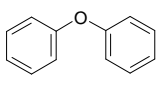
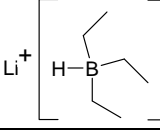
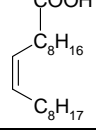
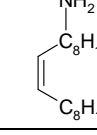
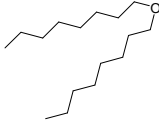
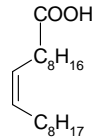
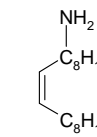
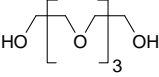
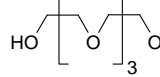
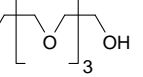
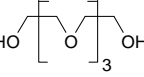
80 Since iron pentacarbonyl is highly flammable and very toxic, alternative methods have soon been developed, in which this Fe precursor was replaced by an ionic iron precursor such as FeCl₂ or Fe(acac)₂. In addition, with the goal to facilitate chemical ordering of the FePt alloy particles during the synthesis, attempts were made to slow down the growth

^a CEA, DRFMC, Nanostructure and Magnetism, 17 rue des Martyrs 38054 Grenoble, France. Fax: 33 4 38 78 51 97; Tel: 33 4 38 78 35 62; E-mail: yves.samson@cea.fr

^b CEA, DRFMC, SPrAM (UMR 5819 CNRS-CEA-UJF), 17 rue des Martyrs 38054 Grenoble, France Fax: 33 4 38 78 50 97; Tel: 33 4 38 78 97 19; E-mail: peter.reiss@cea.fr

† Electronic Supplementary Information (ESI) available: X-Ray diffractograms of as-made and annealed nanoparticles; TEM micrographs and diameter distribution histograms of as-made particles. See <http://dx.doi.org/10.1039/b000000x/>

Table 1 The different chemical syntheses investigated in the present study.

Process	Fe precursor	Pt precursor	solvent	Reducing agent	Stabilizer for Fe	Stabilizer for Pt	Ref.
Fe ⁰ Pt ^{II} dioctylether	Fe(CO) ₅	Pt(acac) ₂					5
Fe ⁰ Pt ^{II} dibenzylether	Fe(CO) ₅	Pt(acac) ₂					9
Fe ^{II} Pt ^{II} diphenylether	FeCl ₂	Pt(acac) ₂					8
Fe ^{-II} Pt ^{II} dioctylether	Na ₂ Fe(CO) ₄	Pt(acac) ₂		Na ₂ Fe(CO) ₄			10
Fe ^{II} Pt ^{II} TEG	Fe(acac) ₂	Pt(acac) ₂					11

kinetics. This led to the development of polyol processes. A kinetic control is indeed easier to achieve in a polyol (ethylene glycol, EG, or tetraethylene glycol, TEG, for example), acting simultaneously as the solvent, the reducing agent and the stabilising ligand.¹¹

In the present study, we compared four hot soap methods and a polyol process using TEG. These five methods are summarised in Table 1. The first process, using Fe⁰ and Pt^{II} in dioctylether, was the first synthesis of FePt nanoparticles described, and is still today the most common in literature. In the second method, dibenzylether acts simultaneously as solvent and reducing agent for the Pt precursor. The third process uses an ionic precursor of iron and therefore requires a strong reducing agent, lithium hydride. In the fourth method, the most recent one, the Pt precursor is reduced by the Fe precursor. Finally, in the polyol process, TEG is at the same time the solvent, the reducing agent and the stabilising ligand. For every method, we will characterize structurally and magnetically as-made and annealed particles, so that we can highlight the major differences between all synthesis reactions.

Experimental

Nanoparticles' preparation by the Fe⁰ Pt^{II} dioctylether method⁵

A stirred mixture of Pt(acac)₂ (197 mg; 0.5 mmol) and 1,2-hexadecanediol (388 mg; 1.5 mmol) in dioctylether (15 mL; 12.105 g) is heated under argon to 100°C with a 12°C/min rate. After 15 minutes at 100°C, all the powder has been dissolved and the solution is slightly yellow coloured. Then a solution of Fe(CO)₅ (196 mg; 1 mmol), oleylamine (134 mg;

0.5 mmol) and oleic acid (141 mg; 0.5 mmol) in dioctylether (5 mL; 4.035 g) is injected into the solution containing Pt(acac)₂ while vigorously stirring. As soon as the reaction temperature comes back to 100°C, temperature is set to 295°C with a 10°C/min rate. After 30 minutes of reflux, the reaction mixture is cooled down to room temperature. Then 80 mL of anhydrous ethanol are added, in order to precipitate the particles. They are centrifuged, then dissolved in toluene (20 mL) containing both stabilising ligands (oleic acid and oleylamine; 50 µL of each). 40 mL of anhydrous ethanol are added for the second precipitation step. After centrifugation, the FePt nanoparticles are dispersed in toluene (20 mL) with both surfactants (50 µL of each). The long-term stability of the obtained black dispersion is more than 1 year without a sign of precipitation.

Nanoparticles' preparation by the Fe⁰ Pt^{II} dibenzylether method⁹

A stirred mixture of Pt(acac)₂ (296 mg; 0.75 mmol) and dibenzylether (15 mL; 15.645 g) is heated under argon from room temperature to 240°C with a 5°C/min rate. When the temperature of the solution reaches 100°C, Fe(CO)₅ (294 mg; 1.5 mmol), oleylamine (1.607 g; 6 mmol) and oleic acid (1.697 g; 6 mmol) are injected. The temperature is then kept at 240°C for 1 hour, raised to 280°C with a 5°C/min rate and maintained at this value for 2 hours. During this reflux stage, a colourless liquid is distilled from reaction mixture. This liquid is composed of toluene and benzaldehyde. The reaction mixture is subsequently cooled down to room temperature and the particles are precipitated by adding 80 mL of anhydrous ethanol. They are purified in the same way as in the Fe⁰ Pt^{II} dioctylether method.

Spectroscopic data of distilled fraction. FTIR: $\nu_{\max}/\text{cm}^{-1}$ 3028, 2922 and 2856 (toluene), 2816 and 2734 (benzaldehyde), 1702vs (CO benzaldehyde), 1596 (benzaldehyde), 1496 (toluene), 1202s (benzaldehyde), 1076, 1030 and 728vs (toluene). NMR: δ_{H} (200 MHz; CDCl_3 ; Me_4Si) 2.24 (s, CH_3 of toluene), 7.06, 7.09, 7.13, 7.15, 7.19, 7.20, 7.26, 7.30, 7.33 (m, aromatic protons of toluene and benzaldehyde), 7.67 (dd, $\text{CH}=\text{CH}-\text{C}-\text{CHO}$), 9.77 (s, $\text{Ar}-\text{CHO}$).

155 Nanoparticles' preparation by the Fe^{II} Pt^{II} diphenylether method⁸

Diphenylether (25 mL; 26.825 g) is molten (m.p. 25-27°C) and then added to $\text{Pt}(\text{acac})_2$ (204 mg; 0.52 mmol), FeCl_2 (104 mg; 0.52 mmol) and 1,2-hexadecanediol (535 mg; 2.07 mmol). The resulting mixture is stirred under argon and heated to 100°C. Oleylamine (139 mg; 0.52 mmol) and oleic acid (150 mg; 0.52 mmol) are added at 100°C, causing the solution turning from yellow to grey. Then reaction mixture is heated to 240°C with a 5°C/min rate, and lithium triethylborohydride solution (1 M in THF; 2.5 mL; 2.5 mmol) is added dropwise. After completed hydride addition, the reaction temperature is increased to 258°C, and kept at this value for 20 min. The solution is cooled down to room temperature, and 90 mL of anhydrous ethanol are added for a first precipitation step. Further purification is carried out as described in the nanoparticles' preparation by the Fe^0 Pt^{II} dioctylether method.

175 Nanoparticles' preparation by the Fe^{II} Pt^{II} dioctylether method¹⁰

Collman's reagent, $\text{Na}_2\text{Fe}(\text{CO})_4 \cdot 5(\text{C}_4\text{H}_8\text{O}_2)$ (173 mg; 0.5 mmol) is mixed with $\text{Pt}(\text{acac})_2$ (197 mg; 0.5 mmol), oleylamine (535 mg; 2 mmol) and oleic acid (565 mg; 2 mmol) in dioctylether (20 mL; 16.140 g). The reaction mixture is stirred under argon and heated from room temperature to 100°C with a 10°C/min rate. The temperature is then kept at this value for 25 min before raising it to 295°C with a 10°C/min rate and maintaining it there for 30 min. After cooling down the reaction mixture to room temperature, anhydrous ethanol (80 mL) is added to achieve precipitation of the particles, followed by the purification as described before (see Nanoparticles preparation by the Fe^0 Pt^{II} dioctylether method).

Nanoparticles' preparation by the Fe^{II} Pt^{II} TEG method¹¹

A reaction flask containing a stirred mixture of $\text{Pt}(\text{acac})_2$ (207 mg; 0.53 mmol), $\text{Fe}(\text{acac})_2$ (134 mg; 0.53 mmol), tetraethylene glycol (28.5 g; 146.7 mmol) and C_{12}E_8 (576 mg) is put into a salt bath at 330°C. The reaction mixture is kept under reflux for 4 h 20 under argon flow. Then it is cooled down to room temperature and the particles are transferred into the toluene phase. For this phase transfer, oleic acid (158 mg) and oleylamine (150 mg) in toluene (60 mL) are added to the reaction mixture. Stirring with a high-speed mechanical stirrer (23 000 rpm for 2 min) results in an emulsion, which decants into an orange TEG and a black toluene phase. The toluene phase is concentrated to 20 mL, then oleic acid and oleylamine (50 μL of each) are added. The resulting dispersion is precipitated a first time by adding anhydrous ethanol (60 mL). Particles are then centrifuged and redispersed in toluene (20 mL) with stabilising ligands (50 μL of each). After a second precipitation step with 40 mL of ethanol, followed by centrifugation, the particles are finally dispersed in toluene (20 mL) containing oleic acid and oleylamine (50 μL of each).

Characterisation methods

IR absorption spectra were recorded on a FTIR-ATR spectrometer (Perkin Elmer Paragon 500). Proton NMR spectroscopy was performed on a Bruker C200 MHz spectrometer. X-Ray diffraction of FePt nanoparticles were obtained in the reflection geometry using an X-ray diffractometer (Philips, X'PERT) at room temperature with $\text{Co K}\alpha$ radiation (wavelength 1.789 Å). FePt nanoparticles were deposited on Silicon wafer substrate by casting and drying the nanoparticles/toluene dispersion. High-resolution TEM micrographs of FePt nanoparticles were obtained using a JEOL 4000EX microscope operated at 400 kV. For TEM studies, a drop of the diluted FePt dispersion was deposited onto a carbon holey grid (ELOISE SARL). Energy dispersive x-ray spectroscopy measurements were obtained using a scanning electron microscope JEOL JSM-840A. The magnetic properties of the FePt nanoparticles samples were determined using a Quantum Design DC Superconducting Quantum Interference Device (DC SQUID; Model MPMS XL) magnetometer.

Table 2 Compositions, structural characteristics (diameters determined from TEM images; fcc cell parameter of FePt solid solution) of as-made FePt nanoparticles.

Method	Av. diameter (dispersion) ^a	Precursors composition ^b	Global composition ^c	a (Å) Core composition ^d	
Fe^0 Pt^{II} dioctylether	3.4 nm (16 %)	$\text{Fe}_{67}\text{Pt}_{33}$	$\text{Fe}_{51}\text{Pt}_{49}$	3.884 Å $\text{Fe}_{32}\text{Pt}_{68}$	core-shell structure (Fe shell: 0.18 nm thick \approx 1 layer)
Fe^0 Pt^{II} dibenzylether	7.4 nm (12 %)	$\text{Fe}_{67}\text{Pt}_{33}$	$\text{Fe}_{28}\text{Pt}_{72}$	3.889 Å $\text{Fe}_{28}\text{Pt}_{72}$	no shell and global composition is not Fe rich enough
Fe^{II} Pt^{II} diphenylether	4.2 nm (14 %)	$\text{Fe}_{60}\text{Pt}_{40}$	$\text{Fe}_{60}\text{Pt}_{40}$	3.887 Å $\text{Fe}_{30}\text{Pt}_{70}$	core-shell structure (Fe shell: < 0.37 nm thick \approx less than 2 layers)
Fe^{II} Pt^{II} dioctylether	3.4 nm (15 %)	$\text{Fe}_{50}\text{Pt}_{50}$	$\text{Fe}_{48}\text{Pt}_{52}$	3.885 Å $\text{Fe}_{31}\text{Pt}_{69}$	core-shell structure (Fe shell: 0.15 nm thick \approx 1 layer)
Fe^{II} Pt^{II} TEG	3.0 nm ^e	$\text{Fe}_{50}\text{Pt}_{50}$	$\text{Fe}_{47}\text{Pt}_{53}$	3.851 Å $\text{Fe}_{46}\text{Pt}_{54}$	no shell but global composition is Fe rich enough

^a Diameters determined from TEM images. ^b Composition given by the molar ratio of metal precursors initially used. ^c Composition obtained through EDX or ICP-AES. ^d fcc cell parameter of the FePt alloy and composition derived from Vegard's law.¹² ^e Diameter of the crystallites determined with X-ray diffraction using Scherrer's formula.

Results and discussion

230 FePt nanoparticles' synthesis

Fe⁰ Pt^{II} dioctylether method: Fe(CO)₅ has a boiling point (103°C), that is far below the reaction temperature (up to 295°C) and therefore the Fe precursor reacts at the liquid-vapour interface within the reaction flask. This virtually reduces the quantity of Fe(CO)₅ available at a given reaction time with respect to the initially introduced quantity. In order to compensate for this "loss" and to get an equimolar final composition, an excess of Fe precursor is used as compared to the Pt one (see precursors' composition in Table 2).

240 The analysis of high-resolution TEM micrographs indicates that particles with an average diameter of 3.4 nm are obtained. XRD reveals that they are made of FePt solid solution. The disordered alloy has a face-centred cubic symmetry, with a cell parameter $a = 3.884 \text{ \AA}$. This value is consistent with a composition Fe₃₂Pt₆₈, according to Végard's law, which describes the cell parameter value of a substitutional solid solution.¹² The composition has to be compared with the global composition we deduced from ICP-AES, Fe₅₁Pt₄₉. The difference between both values is the first indication that suggests a core-shell structure for as-made particles. According to that model, particles are constituted by an iron-depleted core (32 % atomic) surrounded by a shell made of pure iron. This model is only valid if no iron oxide particles, or any second by-product, is present in the analyzed fraction. 255 Indeed, we neither observed any diffraction peaks corresponding to a second phase, nor any iron oxide particles in TEM micrographs. Such particles can be easily recognized with TEM, by measuring the lattice parameter or using the diffraction mode. They also appear less contrasted than FePt particles on the micrographs, since Fe has a significantly lower atomic number Z than Pt.

If we suppose that the FePt nanoparticles are spherical, we can calculate an average shell thickness by comparing the global composition and the core composition. The value we obtain, 0.18 nm, corresponds to one Fe monolayer. This confirms that the X-Ray data are consistent with a core-shell structure: such a thin shell would not give significant XRD contribution. However, it is able to compensate for the iron-depletion of the core because at the nanometer scale, a huge number of atoms are located on the surface. For example, a truncated octahedral shaped particle with 3.3 nm diameter will include a total number of 1289 atoms, among which 502 atoms are located on the surface, i.e. 39 % of the total amount.

1,2-hexadecanediol is considered both as a reducing agent and as a *co-surfactant*,⁸ since it is an amphiphilic molecule.¹³ We performed a synthesis without 1,2-hexadecanediol and found that 4.0 nm diameter FePt particles were formed in this way. In this case, the Pt^{II} precursor is likely reduced by the Fe⁰ precursor, which yields metallic platinum, but also oxidised iron in the Fe^{II} state. Such a reaction, which can easily be explained by the more noble character of Pt, has already been mentioned by Shukla *et al.*¹⁴ A TEM investigation of the particles we prepared without diol is consistent with this hypothesis. We observed a thick iron oxide shell around FePt nanoparticles, as well as some iron oxide particles. The global stoichiometry determined with

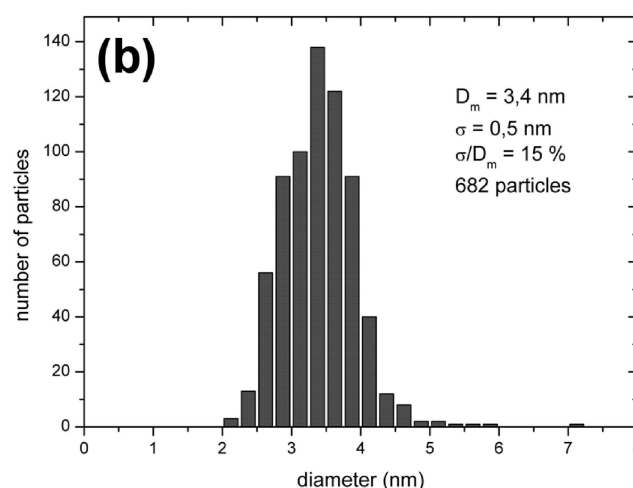
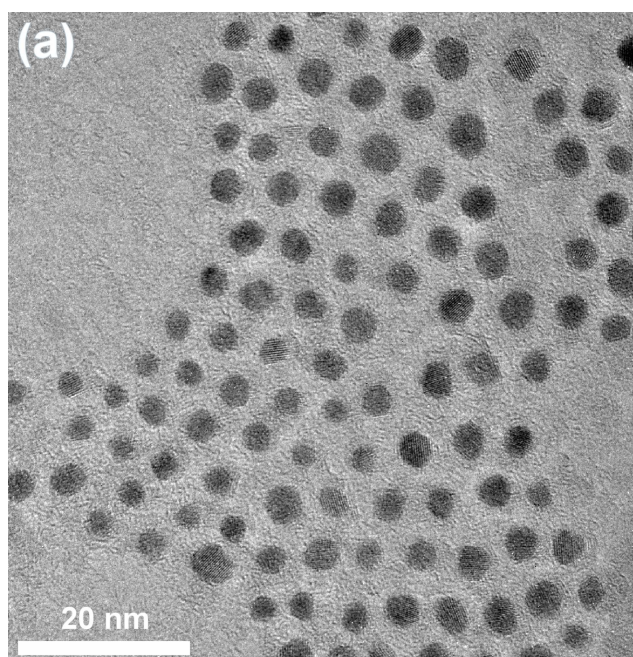


Fig. 1 (a) TEM micrograph of nanoparticles produced by the Fe⁰ Pt^{II} dioctylether method. (b) Diameter distribution of these particles determined from TEM observations.

EDX is Fe₆₀Pt₄₀, whereas the core stoichiometry from XRD measurements accounts for Fe₃₅Pt₆₅. If we assume that all the Pt atoms are present in FePt alloy, we deduce that in a particle composed of 100 atoms, 40 Pt⁰ and 21 Fe⁰ atoms are located in core. As a consequence, there are 39 Fe^{II} atoms left, located in iron oxide shell and separate iron oxide particles. Hence, the amount of metallic Pt is as high as the amount of oxidised Fe. This rough calculation corroborates the assumption that, in absence of 1,2-hexadecanediol, the Pt^{II} precursor oxidises the Fe⁰ precursor.

Fe⁰ Pt^{II} dibenzylether method: In this method, our experimental results suggest that dibenzylether acts simultaneously as the solvent and the reducing agent. We detected the formation of toluene and benzaldehyde during the reaction (cf. Experimental Section). This indicates that the ether bond C–O of dibenzylether underwent a homolytic cleavage yielding mesomery-stabilised benzyl and benzoyl radicals, which most probably play a role in the synthesis

305 reaction. For the elucidation of the detailed mechanism further studies are necessary, which go beyond the scope of the present article.

Like in the previous method: i) an analysis of the global composition by EDX reveals that a significant amount of Fe precursor is lost during the synthesis, ii) XRD results are consistent with an iron-depleted core. Interestingly, we observe that the global composition is the same as the core composition. We infer from this that in this case no Fe shell is present. The exclusion of an additional reducing agent, such as diol or hydride, slows down the nucleation rate and leads to larger particles.

Fe^{II} Pt^{II} diphenylether method: Since this process uses a non volatile Fe precursor and a strong reducing agent, no Fe loss is observed during synthesis. But once again, an iron-depleted core is formed, which is covered by an iron shell. The calculated shell thickness accounts for 2 layers (see Table 2). This value is however probably overestimated due to the presence of a small number of iron oxide nanoparticles visible in TEM micrographs.

Fe^{II} Pt^{II} dioctylether method: In this process, Fe precursor is the reducing agent of Pt^{II} and the reaction can be written schematically:¹⁰ Fe^{-II} + Pt^{II} → Fe⁰ + Pt⁰. Since the transformation of one Pt^{II} cation to the metallic state requires the presence of one Fe^{-II} anion, we expect the formation of homogeneous particles with close to perfect Fe₅₀Pt₅₀ stoichiometry. Heterogeneous nucleation (nucleation of Fe without Pt) should also be avoided in such a process.

Surprisingly, the as-made particles prepared by this method (see Figure 1) also show a core-shell structure with an iron-depleted core, but with a global composition close to Fe₅₀Pt₅₀.

Fe^{II} Pt^{II} TEG method: This way of synthesising FePt nanoparticles is attractive since it is very easy to put into practice: there is no need for additional stabilising ligands and reducing agents and no pyrophoric, volatile or toxic Fe precursor is required. Furthermore, it is likely to provide partially ordered particles because of slower growth kinetics.¹⁵ A major disadvantage of the polyol process is however that it yields highly polydispersed and strongly aggregated particles. We performed a phase transfer from TEG to toluene through an emulsion step, but still the particles were poorly soluble. We also tried polyol reactions in TEG with stabilising ligands, either with C₁₂E₈ (octaethylene glycol monododecylether) or with oleic acid and oleylamine mixed with C₁₂E₈. But none of these experiments provided well-dispersed nanoparticles.

Like in the other method using a cationic Fe^{II} precursor, no Fe loss occurs: the precursors' composition and the global composition are similar. Furthermore, the lattice parameter is significantly lower than in all the other methods. As a result, we do not observe a core-shell structure and particle composition is close to Fe₅₀Pt₅₀.

Magnetic properties (as-grown nanoparticles)

Magnetic measurements provide further insight on the as-grown FePt nanoparticles, with new data that have to be compared with chemical and structural ones to assess the consistency of the analysis here provided.

Let us start with the magnetic anisotropy. This key parameter for any application can be derived from the

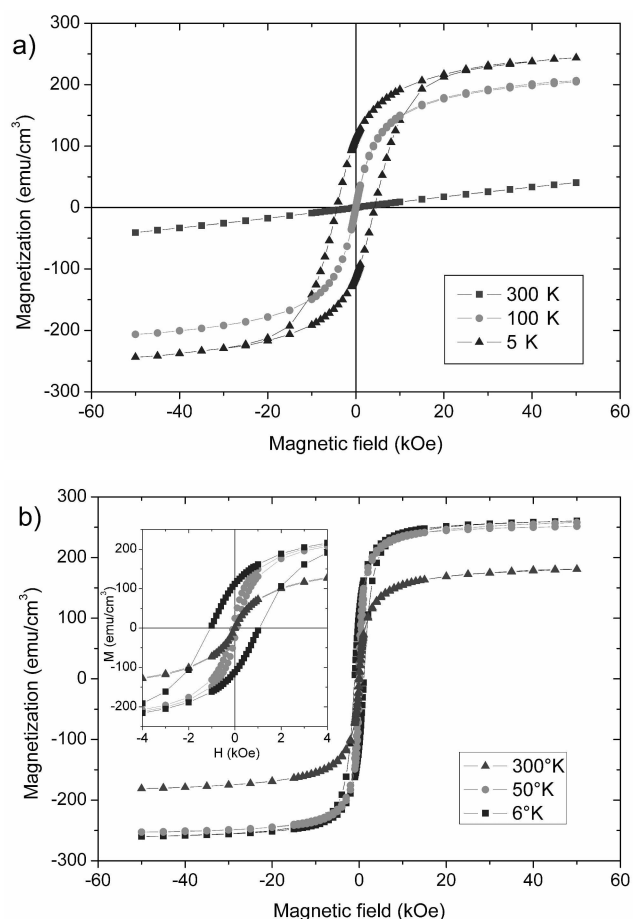


Fig. 2 Magnetic hysteresis loops of FePt nanoparticles prepared with (a) the Fe⁰ Pt^{II} dioctylether method, and with (b) the Fe⁰ Pt^{II} TEG method. The inset restricts to the low field values.

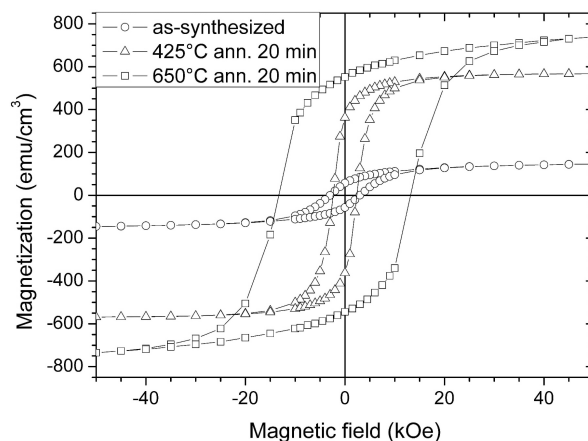


Fig. 3 A series of low-temperature ($T = 6$ K) magnetisation measurement for various annealing temperatures for particles made with the Fe⁰ Pt^{II} dioctylether method.

$$K_u V = k_B T_B \ln(f_0 t_m) \quad (1)$$

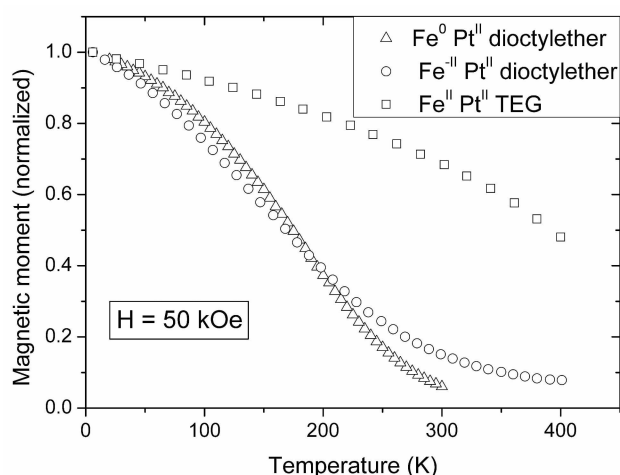


Fig. 4 Magnetisation as a function of temperature for FePt nanoparticles obtained by three chemical synthesis methods.

blocking temperature (T_B). Above T_B , even if the local ferromagnetic alignment of the individual spins is preserved, the magnetic moment of each nanoparticle is randomly reversed by thermal fluctuations. One can write Equation (1) for non-interacting magnetic nanoparticles, where k_B stands for the Boltzmann constant, K_u and V for the magnetic anisotropy and the volume of the nanoparticle respectively. f_0 is the attempt frequency, classically taken as 10^9 Hz, t_m the mean time elapsed between thermally induced reversal events. Here, T_B values are extracted using a classical procedure from the Field Cooled – Zero Field Cooled (FC-ZFC) magnetisation curves obtained with a SQUID magnetometer (Table 3). These values of T_B correspond to a magnetic anisotropy in the 10^5 J/m³ range. Some uncertainty arises from the fact that the mere application of Equation (1) does not take into account the size and anisotropy dispersions of the FePt nanoparticles. However, this uncertainty does not hide the key result: as-grown nanoparticles exhibit anisotropy values roughly one order of magnitude lower than the ones that would be associated to the chemically ordered phase. This result is consistent with the X-Ray data indicating that the as-grown nanoparticles are within the chemically disordered fcc phase.

In addition, we found very low magnetisation values for all as-synthesised FePt nanoparticles, relative to the $Fe_{50}Pt_{50}$ bulk values (1140 emu/cm³ for the $L1_0$ phase) (Table 3). Interestingly, such a low magnetisation (with respect to the

Table 3 Magnetic properties of as-synthesised nanoparticles

	$Fe^0 Pt^{II}$ dioctylether	$Fe^{II} Pt^{II}$ dioctylether	$Fe^{II} Pt^{II}$ TEG
T_B (K) ^a H = 100 Oe	20	14	85
$M_s(6 K)$ (emu/cm ³)	244	185	310
Coercive field H_c (Oe)	4200	1600	1000
Curie temperature (K)	260	280	600
α exponent	1.74	1.36	1.71

^a t_m value fixed at 100 s, the acquisition time of an experimental point for the FC-ZFC curves.

bulk value) has been observed for chemically grown $NiFe_2O_4$ nanoparticles coated with surfactants like oleic acid.¹⁶ The authors proposed that the strong interaction between the surfactants and the surface of the nanoparticle may result in a non-ferromagnetic shell. The same idea has been recently proposed for FePt nanoparticles coated with oleic acid.¹⁷ Within a 3.5 nm diameter nanoparticle, 40 % of the atoms are at the surface. Hence, a pure iron shell (whose existence is suggested by structural data) would mean that 80 % of iron atoms included within a $Fe_{50}Pt_{50}$ nanoparticle are at the surface. If non magnetic, such an Fe shell will then reduce the average magnetisation down to the experimental values. Furthermore, the magnetisation appears higher for the nanoparticles prepared using the $Fe^{II} Pt^{II}$ TEG method. This is perfectly consistent with the absence of a core-shell structure in this latter case, as deduced from the structural data. Once again, a rough quantitative estimation fits well with the measured magnetisation.

The hysteresis loops provide other interesting pieces of information. For the nanoparticles prepared in dioctylether by the $Fe^0 Pt^{II}$ method: At 5 K, below the blocking temperature, it is interesting to see that we do not get the square loop that would be expected from a Stoner Wolfarth model (reversal by coherent rotation of the magnetisation axis).¹⁸ This is likely due to a dispersion in the anisotropy values of the nanoparticles, that lead to a corresponding dispersion of the coercive fields. More detailed simulations indicate that a value of 0.6 for standard deviation (lognormal distribution) of the anisotropy value is required to correctly fit the experimental curve. At 100 K, the hysteresis loop follows quite well the Langevin law describing the evolution of the magnetisation against the field of an assembly of identical and non-interacting magnetic particles at high temperature ($T > T_B$ superparamagnetism behaviour)¹⁹ (Fig. 2a). At 300 K, whereas the magnetisation of nanoparticles produced by TEG method follows a Langevin law (Fig. 2b), a linear variation is observed for the ones prepared by $Fe^0 Pt^{II}$ dioctylether method. Such a linear variation, expected for paramagnetic materials, indicates that the measurement temperature is above or not far from the Curie temperature. More directly, the Curie temperature can be deduced by fitting the $M(T)$ curves obtained under a large applied field (Fig. 3). The law in Equation 2 is derived from the spin wave model that stands far below the Curie temperature. The exponent α generally takes the value 3/2 (Block law) for bulk ferromagnetic materials. For both dioctylether based synthesis (Table 3), we obtain reasonable values for α , and Curie temperatures far below the ones expected at the equiatomic composition (750 K for the $L1_0$ phase, ~ 600 K for the fcc phase). According to the published phase diagram of the FePt alloy,²⁰ a Curie temperature in the 300 K range would correspond to a $Fe_{30}Pt_{70}$ composition (close to the composition values of the nanoparticles cores deduced from XRD data, see Table 2). Conversely, the Curie temperature is clearly far higher for the nanoparticles prepared by the TEG method (Fig. 3). This is consistent with an iron richer composition of the nanoparticle

$$M = M_s(1 - BT^\alpha) \quad (2)$$

core, as expected in the absence of a core-shell structure.

XPS study

An XPS study (see Figure 5a and Table 4) reveals that as-made particles include only one type of Pt atoms. Pt 4f 7/2 binding energy corresponds to Pt⁰. Similarly, only one kind of Fe atom can be observed (see Figure 5b), and Fe 2p 3/2 binding energy corresponds to Fe^{III}. These oxidised Fe atoms are those from the iron outer shell, and their oxidation state explains why they are non magnetic.

In order to probe the core of particles, we conducted Ar sputtering experiments. As shown by Table 4, the molar ratio Fe/Pt decreases after Ar sputtering, which indicates that more Fe atoms were etched than Pt atoms. Then, two types of Fe atoms are detected after etching: Fe⁰ from core (38 %) and Fe^{III} from shell (62 %). It is in accordance with a core-shell structure including a core made of Pt⁰ and Fe⁰, and a shell only made of Fe^{III}. That is the reason why we still observe only one kind of Pt atoms after etching, corresponding to Pt⁰ from core. Non-oxidised Fe atoms from core cannot be seen without etching because the probe depth with the XPS technique is not large enough.

As a conclusion, both magnetic properties and XPS studies indicate a core-shell structure for as-made FePt nanoparticles prepared by the three following methods: Fe⁰ Pt^{II} dioctylether, Fe^{II} Pt^{II} diphenylether and Fe^{-II} Pt^{II} dioctylether. The shell is likely to consist of iron oxide (non magnetic iron in the Fe^{III} state) and is too thin to be seen on TEM micrographs and to generate a significant XRD signal. Such a non magnetic shell has already been mentioned in literature and was called *dead layer*: Wu *et al* attributed the low magnetisation state of this layer to bonds between carbonyl groups of oleic acid and Fe.²¹ Anders *et al* carried out a NEXAFS study on FePt nanoparticles and showed that a very thin layer of oxide (0.4 nm) surrounding particles is sufficient to explain the observed spectra.²² Finally, a Mössbauer study by Stahl *et al.* indicates two types of Fe atoms in as-made FePt nanoparticles prepared with Fe⁰ Pt^{II} dioctylether method.²³

Now let us focus on the availability of the Fe atoms of the shell: are they able to take part in the building of the ordered phase? If it is not, core-shell particles will remain iron-depleted after chemical ordering. Conversely, if Fe atoms from the shell can diffuse into core, the transition phase of particles will lead to the equimolar ordered phase L1₀. This is obviously a key point for the targeted application of FePt nanoparticles in data storage.

Annealing experiments

The diagram phase of FePt alloy indicates that for

Table 4 Argon etching experiment on nanoparticles prepared with the Fe⁰ Pt^{II} dioctylether method. These experiments were monitored with X-Ray Photoelectron Spectroscopy.

	before Ar sputtering	after Ar sputtering ^a
molar ratio Fe/Pt	1.04	0.63
binding energy (eV) Pt 4f 7/2	71.3	71.4
binding energy (eV) Fe 2p 3/2	710.8 (100 %)	707.4 (38 %) 709.7 (62 %)

^a Ar with 3 keV energy, 10⁻⁶ mbar, 15 min.

compositions between Fe₄₄Pt₅₆ and Fe₆₂Pt₃₈, chemical ordering will lead to L1₀ phase. On the other hand, particles with iron-depleted compositions ranging from Fe₂₀Pt₈₀ to Fe₄₀Pt₆₀ will generate L1₂ ordered phase showing one Fe atom for three Pt atoms. As a consequence, if Fe atoms from shell are not available, a core-shell FePt nanoparticle will yield a particle made of a L1₂ phase core, covered with an iron oxide

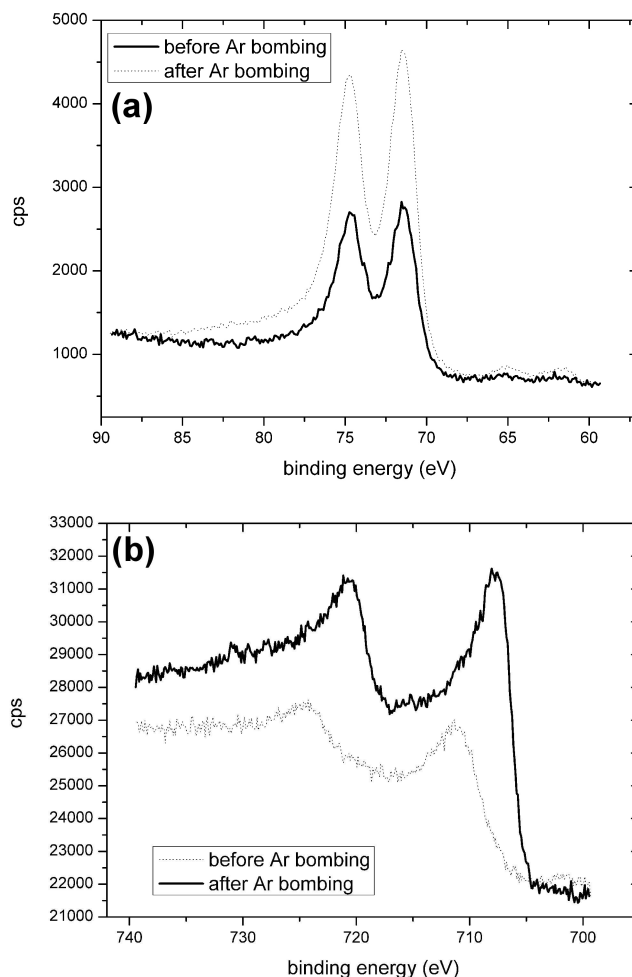


Fig. 5 X-Ray photoelectron spectroscopy of nanoparticles prepared with the Fe⁰ Pt^{II} dioctylether method. (a) Pt 4f 7/2 peaks of particles before and after Ar sputtering. (b) Fe 2p 3/2 peaks of particles before and after Ar sputtering.

Table 5 Chemically ordered phases obtained after annealing the nanoparticles (650°C, 1 h, under vacuum) deposited on SiO₂ substrates.

Process	Global composition	Ordered phase Cell parameters ^a (Å)
Fe ⁰ Pt ^{II} dioctylether	Fe ₅₁ Pt ₄₉	L1 ₀ $a = 3.859; c = 3.736$
Fe ⁰ Pt ^{II} dibenzylether	Fe ₂₈ Pt ₇₂	Disordered FePt + L1 ₂ $a = 3.868$
Fe ^{II} Pt ^{II} diphenylether	Fe ₆₀ Pt ₄₀	L1 ₀ $a = 3.839; c = 3.711$
Fe ^{-II} Pt ^{II} dioctylether	Fe ₄₈ Pt ₅₂	L1 ₀ $a = 3.862; c = 3.726$
Fe ^{II} Pt ^{II} TEG	Fe ₄₇ Pt ₅₃	L1 ₀ $a = 3.859; c = 3.737$

^a L1₀ phase is face centred tetragonal, L1₂ phase is face centred cubic.

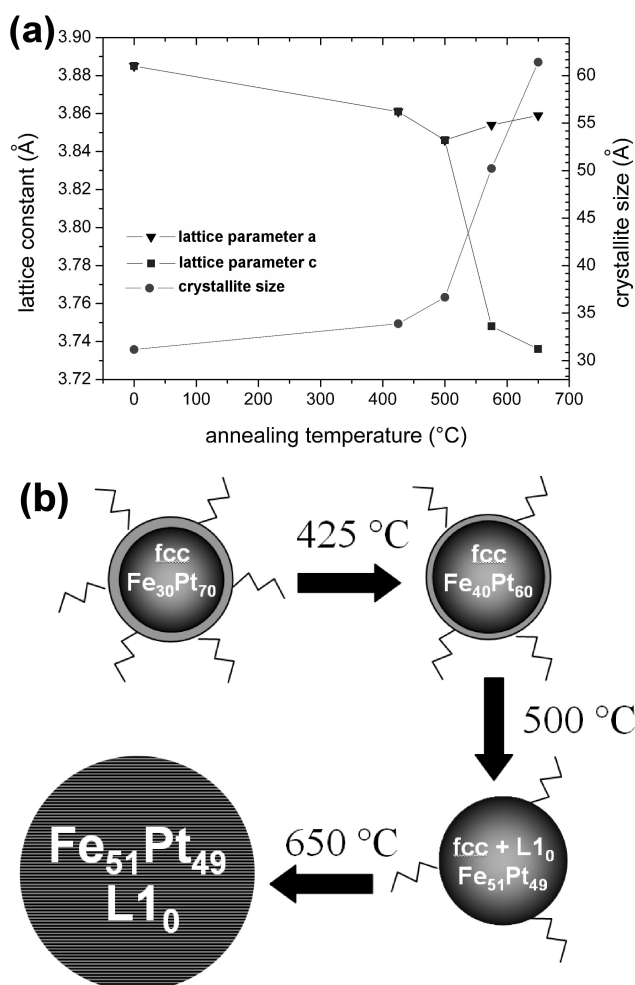


Fig. 6 (a) These curves plot lattice constants (*a* and *c*) and crystallite size versus temperature for FePt nanoparticles annealed 2 hours under vacuum (particles made with the $Fe^0 Pt^{II}$ dioctylether method). (b) This scheme represents the diffusion of Fe atoms from shell into core, so as to take part into the building of L1₀ phase. The compositions indicated on particles are core compositions deduced from lattice constant.

shell.

Table 5 gathers results for the annealing processes of all particles, which consisted in a heating treatment under vacuum (10^{-5} to 10^{-6} mbar). All the particles having a global composition between Fe₄₇Pt₅₃ and Fe₆₀Pt₄₀ produced L1₀ phase, thereby proving the ability for Fe atoms from shell to diffuse. As expected, particles prepared with $Fe^0 Pt^{II}$ dibenzylether method yielded L1₂ phase. They have indeed an iron-depleted global composition.

We monitored the transition phase by means of XRD, as shown in Figure 6a, for particles synthesised with $Fe^0 Pt^{II}$ dioctylether method. The transition phase between disordered

fcc solid solution and ordered fct phase L1₀ occurs when lattice constant *a* splits into *a* and *c* parameters, *i.e.* at about 500 °C. Interestingly, we notice a downward trend of the lattice constant *a* before splitting. The same tendency has also been reported recently by Nakaya *et al.*²⁴ but no explanation was given. We think that below 500 °C the diffusion of Fe atoms from the shell into the core causes an iron enrichment of the disordered solid solution (see Figure 6b). Since Fe atoms are smaller than Pt atoms, this enrichment leads to a lower value of the lattice constant *a*. Around 500 °C, the phase transition occurs but sintering cannot be avoided, the crystallite size then strongly increases.

The fact that Fe atoms would diffuse – at a moderate temperature (425 K) – from the outer shell towards the alloyed core of the nanoparticles finds further support from the magnetic experiments. Indeed, after a 20 min. annealing at 425 °C, we observe a large increase of *M_s*. Interestingly, the absence of a significant increase of the coercive field suggests that the anisotropy of the nanoparticles does not strongly increase in the same time (fig. 6). Quantitatively, the increase on the overall magnetisation may be partly induced by the thermal decomposition of the surfactants present at the nanoparticles' surface¹⁷ (the surfactants being suspected to render the shell non magnetic), in addition to the Fe diffusion within the core. After annealing at a higher temperature (650 °C), the coercivity *H_c* increases from 4200 Oe (as-grown nanoparticles) to 13 kOe. This is consistent with the obtention of the large anisotropy - L1₀ phase.

In summary, the structural and magnetic studies as well as the annealing experiments support the model of a core-shell structure of the as-prepared FePt nanoparticles. The formation of this structure can be explained by the difference of kinetics between the two following reactions: the reduction of Pt^{II} to Pt⁰, and the transformation of the Fe precursor into metallic Fe. The nucleation of Pt is much easier to trigger, that is why the formation of FePt nanoparticles occurs via a Pt-rich core, followed by a slower deposition of Fe and Pt atoms. This two-step growth mechanism has been recently reported in literature for both methods relying on the reduction of Pt(acac)₂ and decomposition of Fe(CO)₅,⁹ and a process involving the pyrolysis of Fe(OEt)₃ and Pt(acac)₂.²⁵ Interestingly, we notice that this difference of kinetics leads to a core composition around Fe₃₀Pt₇₀ (see Table 2), whatever hot soap method is used, *i.e.* the core compositions of the particles are similar although the chemical mechanisms involved in these four syntheses are completely different. The polyol process TEG is the only preparation method among those studied which does not follow this two-step growth mechanism.

In the case of rather small particles (4 nm diameter and

Table 6 Syntheses of larger FePt nanoparticles: structural data about as-made particles and ordered phase obtained from annealing.

Process	Surfactant (equivalents) ^a	Av. diameter (nm)	Precursors composition	Global composition	<i>a</i> (Å) Core composition	Ordered phase Lattice parameters (Å)
Fe ⁰ Pt ^{II} dioctylether	1.5	3.4 (16 %)	Fe ₆₇ Pt ₃₃	Fe ₅₁ Pt ₄₉	3.884 (Fe ₃₂ Pt ₆₈)	L1 ₀ (<i>a</i> = 3.859; <i>c</i> = 3.736)
	8	5.0 (7 %)	Fe ₆₇ Pt ₃₃	Fe ₃₉ Pt ₆₁	3.893 (Fe ₂₆ Pt ₇₄)	L1 ₂ (<i>a</i> = 3.867)
Fe ^{II} Pt ^{II} dioctylether	4	3.4 (15 %)	Fe ₅₀ Pt ₅₀	Fe ₄₈ Pt ₅₂	3.885 (Fe ₃₁ Pt ₆₉)	L1 ₀ (<i>a</i> = 3.862; <i>c</i> = 3.726)
	8	4.9 (20 %)	Fe ₅₀ Pt ₅₀	Fe ₂₉ Pt ₇₁	3.899 (Fe ₂₁ Pt ₇₉)	L1 ₂ (<i>a</i> = 3.854)

^a Number of equivalents of oleic acid (compared to the amount of Pt precursor) = number of equivalents of oleylamine.

less), the iron surface can compensate the iron-depletion of the core, so that the global composition is close to equimolar. Since the surface iron is available during subsequent annealing, the core-shell structure does not hinder the formation of the L1₀ phase. With the goal to verify if this is true also for bigger particles, we carried out syntheses with higher amounts of the stabilising ligands (Table 6), leading to lower nucleation rates and larger particle diameters. EDX and X-ray analyses reveal that the as-made particles also exhibit a core-shell structure, with an iron-depleted core and a shell made of iron. Compared to smaller particles, large diameter samples have a larger core and approximately the same shell thickness, therefore they have an iron-depleted global composition. That is the reason why they yield the L1₂ ordered phase after annealing and not the L1₀ one.

Conclusions

We conducted a comparative study on FePt nanoparticles prepared in solution with five different chemical methods. We evidenced by X-ray diffraction and EDX analysis that four of them yielded particles with a core-shell structure consisting of a Pt rich core and a 1-2 monolayers thick Fe shell. The formation of the core/shell structure has its origin in the difference between the nucleation kinetics of Pt and Fe: Pt is much easier to nucleate and faster to deposit on the seeds. Our study is the first one to stress that all the hot soap methods provide particles having very similar core compositions (close to 30 % at. Fe), though very different chemical reactions are involved in these syntheses. Noteworthy even the method relying on the reduction of Pt^{II} by Fe^{II} did not provide homogeneous particles.

We evidenced however that the iron atoms of the shell are available for the formation of the L1₀ phase in the case of small nanoparticles with equimolar global composition. On the contrary, bigger particles yield the L1₂ phase upon annealing.

A completely different synthesis reaction, of the polyol process, exhibits some distinct differences from the hot soap methods: it yields homogeneous particles having an equimolar global composition. Serious drawbacks of this method are however the small size, the high polydispersity and the poor dispersibility of the formed particles.

A common feature of all hot soap methods is that they use oleylamine as stabilising ligands for Pt atoms and oleic acid as ligands for Fe. The amount of oleylamine in the initial reaction mixture controls the nucleation of Pt, likewise oleic acid controls the nucleation of Fe. With the goal to synthesise bigger equimolar FePt nanoparticles and to overcome the problem of core-shell structure formation, novel combinations of ligands should be investigated in further studies, reducing the difference of the reaction kinetics of the two metal precursors. Furthermore, the control over the interaction between the surfactant and the metal precursor is one of the key issues for the synthesis of new particle shapes.²⁶

Reactions involving new ligand molecules such as polyamines, nitriles or thiols are currently under investigation in our laboratory. In order to strengthen the interaction between Pt and its associated ligand, we are currently

investigating syntheses in which oleylamine is replaced by other ligands (such as polyamine, nitrile or thiol).

Acknowledgements

We are indebted to Dr Pierre Delichère for his very helpful XPS experiments. Assistance by Dr Pascale Bayle-Guillemaud for TEM experiments and by Dr Isabelle Schuster for X-ray diffraction analyses is gratefully acknowledged. This work was supported by French Research National Agency (ANR project CAMAIEU).

Notes and references

- (a) T. Hyeon, *Chem. Commun.*, 2003, 927-934 (b) B. L. Cushing, V. L. Kolesnichenko and C. J. O'Connor, *Chem. Rev.*, 2004, **104**, 3893-3946 (c) C. Desvaux, C. Amiens, P. Fejes, P. Renaud, M. Respaud, P. Lecante, E. Snoeck and B. Chaudret, *Nat. Mater.*, 2005, **4**, 750-753. (d) S. Sun, *Adv. Mater.*, 2006, **18**, 393-403 (e) D. L. Huber, *Small*, 2005, **1**, 482-501.
- (a) H. Kodama, S. Momose, N. Ihara, T. Uzamaki and A. Tanaka, *Appl. Phys. Lett.*, 2003, **83**, 5253-5255 (b) S. B. Darling, N. A. Yufa, A. L. Cisse, S. D. Bader and S. J. Sibener, *Adv. Mater.*, 2005, **17**, 2446-2450 (c) S. B. Darling and S. D. Bader, *J. Mater. Chem.*, 2005, **15**, 4189-4195 (d) Q. Guo, X. Teng, and H. Yang, *Adv. Mater.*, 2004, **16**, 1337-1341.
- H. Kodama, S. Momose, T. Sugimoto, T. Uzamaki and A. Tanaka, *IEEE Trans. Magn.*, 2005, **41**, 665-669.
- (a) Q. A. Pankhurst, J. Connolly, S. K. Jones and J. Dobson, *J. Phys. D: Appl. Phys.*, 2003, **36**, R167-R181 (b) X. Gao, K. Tam, K. M. Kerry Yu and S. C. Tsang, *Small*, 2005, **1**, 949-952.
- S. Sun, C. B. Murray, D. Weller, L. Folks and A. Moser, *Science*, 2000, **287**, 1989-1992.
- E. V. Shevchenko, D. V. Talapin, A. L. Rogach, A. Kornowski, M. Haase and H. Weller, *J. Am. Chem. Soc.*, 2002, **124**, 11480-11485.
- S. S. Kang, D. E. Nikles and J. W. Harrell, *J. Appl. Phys.*, 2003, **93**, 7178-7180.
- S. Sun, *Us. Pat.*, 6 676 729, 13 january 2004.
- M. Chen, J. P. Liu and S. Sun, *J. Am. Chem. Soc.*, 2004, **126**, 8394-8395.
- L. E. M. Howard, H. Loc Nguyen, S. R. Giblin, B. K. Tanner, I. Terry, A. K. Hughes and J. S. O. Evans, *J. Am. Chem. Soc.*, 2005, **127**, 10140-10141.
- B. Jeyadevan, K. Urakawa, A. Hobo, N. Chinnasamy, K. Shinoda, K. Tohji, D. D. J. Djayaprawira, M. Tsunoda and M. Takahashi, *Jpn. J. Appl. Phys.*, 2003, **42**, L350.
- A. Bonakdarpour, J. Wenzel, D. A. Stevens, S. Sheng, T. L. Monchesky, R. Löbel, R. T. Atanasoski, A. K. Schmoekkel, G. D. Vernstrom, M. K. Debe and J. R. Dahn, *J. Electrochem. Soc.*, 2005, **152**, A61-A72.
- G. Weidemann, G. Brezesinski, D. Vollhardt, C. DeWolf and H. Möhwald, *Langmuir*, 1999, **15**, 2901-2910.
- N. Shukla, C. Liu and A. G. Roy, *Mater. Lett.*, 2006, **60**, 995-998.
- B. Jeyadevan, A. Hobo, K. Urakawa, C. N. Chinnasamy, K. Shinoda and K. Tohji, *J. Appl. Phys.*, 2002, **93**, 7574-7576.
- A. E. Berkowitz, J. A. Lahut, I. S. Jacobs, and Lionel M. Levinson, *Phys. Rev. Lett.*, 1975, **34**, 594-597
- X. W. Wu, C. Liu, L. Li, P. Jones, R. W. Chantrell, and D. Weller, *J. Appl. Phys.*, 2004, **95**, 6810-6812.
- E. C. Stoner and E. P. Wohlfarth, *Phil. Trans. Roy. Soc.*, 1948, **A240**, 599-642
- C. P. Bean and J. D. Livingston, *J. Appl. Phys.*, **30 Suppl.**, 120S-129S.
- A. Kussman and G. V. Rittberg, *Z. Metallk. Metallforsch.*, 1950, **41**, 470
- X. W. Wu, C. Liu, L. Li, P. Jones, R. W. Chantrell and D. Weller, *J. Appl. Phys.*, 2004, **95**, 6810-6812.
- S. Anders, M. F. Toney, T. Thomson, J.-U. Thiele, B. D. Therriis, S. Sun and C. B. Murray, *J. Appl. Phys.*, 2003, **93**, 7343-7345.

-
- 23 B. Stahl, N. S. Gajbhiye, G. Wilde, D. Kramer, J. Ellrich, M. Ghafari, H. Hahn, H. Gleiter, J. Weissmüller, R. Würschum and P. Schlossmacher, *Adv. Mater.*, 2002, **14**, 24-27.
- 24 M. Nakaya, M. Kanehara and T. Teranishi, *Langmuir*, 2006, **22**, 3485-3487.
- 25 S. Saita and S. Maenosono, *Chem. Mater.*, 2005, **17**, 6624-6634.
- 26 (a) N. Shukla, E. B. Svedberg, J. Ell and A. J. Roy, *Mater. Lett.*, 2006, **60**, 1950-1955 (b) M. Chen, J. Kim, J. P. Liu, H. Fan and S. Sun, *J. Am. Chem. Soc.*, 2006, **128**, 7132-7133.